

## A TWO-SCALE NUMERICAL APPROACH TO GRANULAR SYSTEMS

M. NITKA<sup>1</sup>, J. TEJCHMAN<sup>2</sup>

A two-scale numerical homogenization approach was used for granular materials. At small-scale level, granular micro-structure was simulated using the discrete element method. At macroscopic level, the finite element method was applied. An up-scaling technique took into account a discrete model at each Gauss integration point of the FEM mesh to derive numerically an overall constitutive response of the material. In this process, a tangent operator was generated with the stress increment corresponding to the given strain increment at the Gauss point. In order to detect a loss of the solution uniqueness, a determinant of the acoustic tensor associated with the tangent operator was calculated. Some elementary geotechnical tests were numerically calculated using a combined DEM-FEM technique.

*Key words:* discrete element method, finite element method, granular material, homogenization technique, two-scale approach.

## 1. INTRODUCTION

Granular materials have a discrete and heterogeneous nature. To realistically capture their behaviour, micro-structure should be taken into account at the micro-scale. However, when modelling micro-structure using the FEM, a huge number of finite elements and computational effort are needed. To practically solve this problem, multi-scale computational homogenization approaches are applied (MIEHE et al. [1], FEYEL and CHABOCHE [2], TERADA and KIKUCHI [3], GHOSH et al. [4], KOUZNETSOVA et al. [5], GITMAN et al. [6], MASSART et al. [7]) which are aimed at calculations of material properties at one level using information from different lower levels. In a two-scale approach, the material behaviour is simultaneously studied at two different scales: 1) at the micro-level, where the material micro-structure is distinguished and 2) at the macro-level, where the material is treated as a homogeneous one. These two different scales interact by coupling kinematics, various stresses and forces. Modelling procedures do not lead to closed-form overall constitutive equations but compute a stress-strain

---

<sup>1</sup> Gdańsk University of Technology, Civil and Environmental Engineering Department, Gdańsk, Poland, e-mail: micnitka@pg.gda.pl

<sup>2</sup> Gdańsk University of Technology, Civil and Environmental Engineering Department, Gdańsk, Poland, e-mail: tejchmk@pg.gda.pl

relationship at every integration point of interest of the macro-component by detailed modelling of the microstructure attributed to this point. Thus, they do not require any constitutive assumption at the macro-level by introducing the detailed micro-structure into a macroscopic level. Different modelling techniques can be used at the micro-level, e.g. the finite element method (FEYEL and CHABOCHE [2], KOUZNETSOVA et al. [5]), the Voronoi cell method (GHOSH et al. [4]), numerical methods based on Fast Fourier Transforms (MICHEL et al. [8]), variational multiscale methods (HUND and RAMM [9]), the adaptive heterogeneous multiscale method (ECKARDT and KÖNKE [10]), the method presented by IBRAHIMBEGOVIĆ et al. [11], multi-grid methods (KACZMARCZYK et al. [12]) and finally the so-called coupled volume approach (GITMAN et al. [6]) in which the size of a macro-element is equal to the size of a micro-element to avoid any assumption of the Representative Volume Element (RVE) which is the most important parameter in multi-scale approaches, i.e. it denotes the cell size of the micro-level. The concept of RVE was introduced to determine the corresponding effective properties of a homogenized macroscopic model. The RVE was originally defined by HILL [13] as “a sample that is structurally entirely typical of the whole mixture on average and contains a sufficient number of inclusions for the apparent overall moduli to be effectively independent of the surface values of traction and displacement, as long as these values are macroscopically uniform”. Thus, the size of RVE should be large enough with respect to an individual grain size in order to define overall quantities such as stress and strain, but this size should also be small enough in order not to hide macroscopic heterogeneity (EVESQUE [14]). Recently, GITMAN [15] and SKARŻYŃSKI and TEJCHMAN [16], [17] have shown that the representative volume element (RVE) cannot be defined in softening materials with a standard averaging approach due to occurrence of localized zones whose width is not scaled with the specimen size (the shape of the stress-strain curve strongly depends on the specimen size beyond the elastic region).

The concept of computational homogenization can be summarized as follows (Gitman et al. [6]), Fig.1:

- a) the material is described as homogeneous with effective properties – it does not require any constitutive assumption (macro-level),
- b) a micro-level unit cell (RVE) is assigned to each integration point of the discretized macro-level (down-scaling) and the macro-level strain field is translated into micro-level displacement boundary conditions,
- c) the material is described as heterogeneous with micro-structure and a boundary value problem is solved for each micro-level unit cell with boundary conditions from the macro-level output (micro-level),
- d) homogenization is performed on the micro-level in terms of reaction forces and stiffness relations which provides in effective properties of a homogeneous material to be transferred to the macro-level (up-scaling).

Our study considers a two-scale and two-dimensional numerical homogenization scheme for a description of the behaviour of granular materials (NITKA [18], NITKA et al. [19]). At the micro-scale level, the granular structure is described by rigid interacting

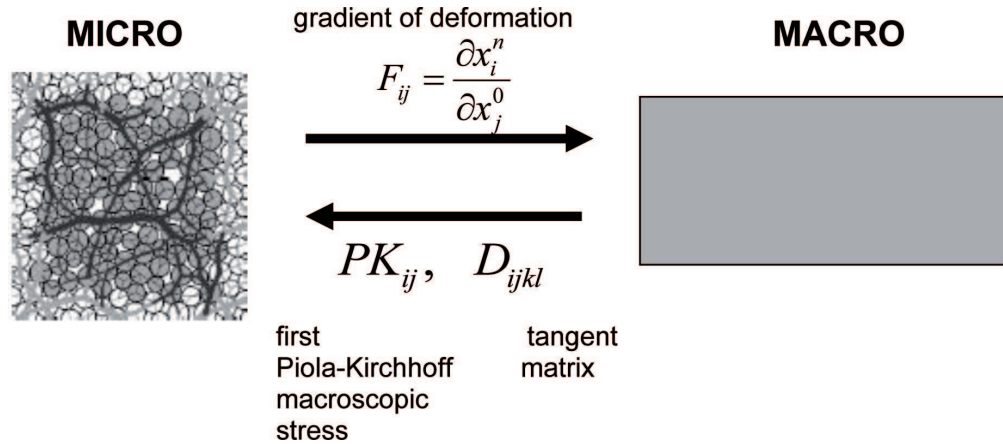


Fig. 1. Computational homogenization using discrete element method (DEM) at micro-level and finite element method (FEM) at macro-level.

Rys. 1. Numeryczna homogenizacja z użyciem metody elementów dyskretnych (MED) na poziomie mikro i metody elementów skończonych (MES) na poziomie makro

discs modelled by the discrete element method (DEM). At the macro-scale level, a numerical solution is obtained with the finite element method (FEM) by means of the tangent stiffness matrix based directly on a discrete behaviour of the granulate. Using the computational homogenization (which links both scales), the average stress response of the granular micro-structure is obtained in each macroscopic Gauss point of the FE mesh as the result of the macroscopic deformation history imposed on REV. In addition, the acoustic tensor is calculated at the Gauss point, which is the best indicator for the unstable material behaviour. The influence of different parameters on the stability of the macroscopic response is presented with numerical tests. Finally, the two-scale DEM-FEM results are depicted for some elementary geotechnical tests such as: an oedometer, a shear and a biaxial compression test.

## 2. MACRO-MICRO LINK

### 2.1. MACROSCOPIC CONSTITUTIVE LAW

For a given history of the deformation gradient, a global stress response of REV is first calculated (Fig.2). The macroscopic stresses from the average formula of inter-granular forces between discs in contact are

$$(2.1) \quad \sigma_{ij} = \frac{1}{S} \sum_{c=1}^{N_c} f_i^c l_j^c \text{ with } i, j \in \{x, y\},$$

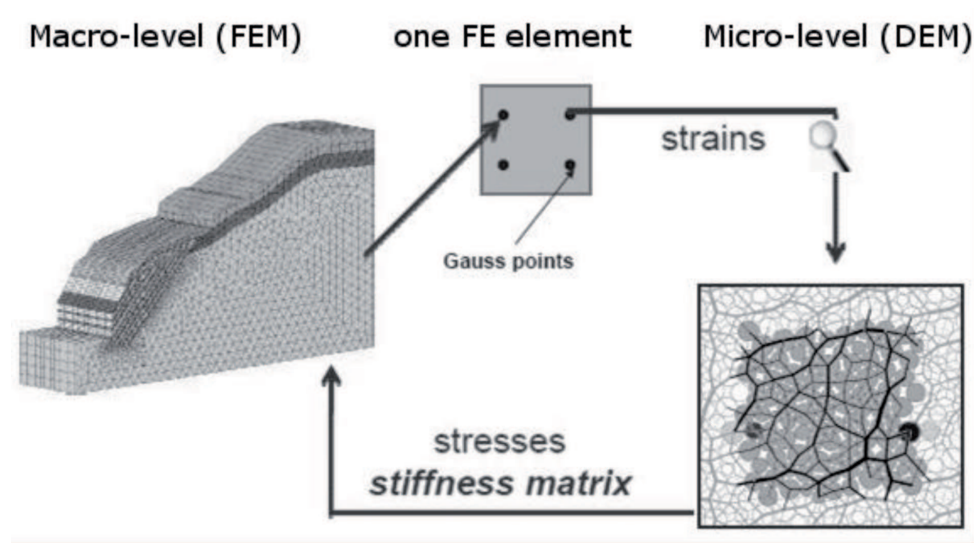


Fig. 2. Schematic representation of two-scale approach for bodies with granular micro-structure.  
 Rys. 2. Schematyczny opis podejścia dwuskalowego dla ciał z granulowaną mikro-strukturą

where  $S$  is the area of the specimen,  $f_i^c$  and  $l_j^c$  are respectively the components of forces acting along the disc contact  $c$  and the component  $j$  of the branch vector joining the centres of two discs in contact (LOVE [20]). Next, the Cauchy stress tensor of Eq.2.1 is converted into the Piola-Kirchhoff stress tensor (BONNET and WOOD [21]) which depends on the history of the deformation gradient

$$(2.2) \quad \bar{\mathbf{P}}(t) = \Gamma' \{ \bar{\mathbf{F}}(\tau), \tau \in [0, t] \}.$$

For any history of the tensor  $\bar{\mathbf{F}}$ , the tensor  $\bar{\mathbf{P}}$  admits the right time derivative tensor  $\dot{\bar{\mathbf{P}}}$  with respect to time  $t$

$$(2.3) \quad \dot{\bar{\mathbf{P}}} = \lim_{\delta t \rightarrow 0} \frac{\bar{\mathbf{P}}(t + \delta t) - \bar{\mathbf{P}}(t)}{\delta t}$$

and for the given history of the tensor  $\bar{\mathbf{F}}$  till the time  $t$ , the right-sided derivative tensor  $\dot{\bar{\mathbf{P}}}$  depends on the right time derivative tensor  $\dot{\bar{\mathbf{F}}}$  only

$$(2.4) \quad \dot{\bar{\mathbf{P}}} = \Theta(\dot{\bar{\mathbf{F}}}),$$

where the function  $\Theta$  is generally non-linear with respect to its argument  $\dot{\bar{\mathbf{F}}}$ . The study is limited to the case, when the history of  $\bar{\mathbf{F}}$  is given by the expression  $\bar{\mathbf{F}} = \mathbf{I} + \alpha \mathbf{G}^0$  with  $\mathbf{G}^0$  being the fixed tensor and  $\alpha$  being the time-like loading parameter (which

changes monotonously from 0 to 1). In this case, the tensor is  $\dot{\mathbf{P}} = \Xi(\alpha)$  and after differentiating with respect to the parameter  $\alpha$ , the tensor  $\dot{\mathbf{F}} = \mathbf{G}^0$ . According to the definition of the function  $\Theta$  (Eq.2.4), an approximate formula can be used (BILBIE et al. [22])

$$(2.5) \quad \Theta(\mathbf{G}^0) \approx \frac{\Xi(\alpha + \Delta\alpha) - \Xi(\alpha)}{\Delta\alpha},$$

which allows one to determine a macroscopic response.

## 2.2. MACROSCOPIC STABILITY

The loss of uniqueness for rate-type boundary value problems is analyzed by the standard Rice's approach (RICE [23]). Following this analysis, the rate of deformation gradient  $\dot{\mathbf{F}}$  is searched which is discontinuous along the boundary of a localized zone

$$(2.6) \quad \dot{F}_{kL}^1 = \dot{F}_{kL}^0 + q_k N_L,$$

where the vector  $\mathbf{N}$  is the normal to a localized zone ( $\|\mathbf{N}\| = 1$ ), the tensor  $\dot{\mathbf{F}}^1$  occurs on the same side as  $\mathbf{N}$  and the tensor  $\dot{\mathbf{F}}^0$  on the opposite side. The stress vector has to be continuous across the interface

$$(2.7) \quad \left( \dot{P}_{ij}^1 - \dot{P}_{ij}^0 \right) N_j = 0.$$

Since  $\dot{P}_{ij}^1$  and  $\dot{P}_{ij}^0$  are linked to  $\dot{F}_{ij}^1$  and, respectively,  $\dot{F}_{ij}^0$  by Eq.2.3, the unknowns  $\mathbf{q}$  and  $\mathbf{N}$  have to satisfy the equation

$$(2.8) \quad \left( \Theta_{ij} \left( \dot{\mathbf{F}}^0 + \mathbf{q} \otimes \mathbf{N} \right) - \Theta_{ij} \left( \dot{\mathbf{F}}^0 \right) \right) N_j = 0$$

for the given tensor  $\dot{\mathbf{F}}^0$ .

In the considered macroscopic quasi-static deformation process, the question of the ellipticity loss therefore reduces to the determination of the value  $\alpha$  for which Eq.2.8 has a non-trivial solution  $\mathbf{q} \neq \mathbf{0}$ . The search of a non-trivial solution is restricted to the case with the tensor  $\dot{\mathbf{F}}^1$  closed to  $\dot{\mathbf{F}}^0$ . By assuming that the function  $\Theta$  is differentiable at  $\dot{\mathbf{F}}^0$ , Eq.2.8 yields after linearization

$$(2.8) \quad D_{ijkl} \left( \dot{\mathbf{F}}^0 \right) q_k N_L N_j = 0,$$

where

$$(2.10) \quad D_{ijkl} \left( \dot{\mathbf{F}}^0 \right) = \frac{\partial \Theta_{ij}}{\partial F_{kl}} \Big|_{\dot{\mathbf{F}}=\dot{\mathbf{F}}^0}.$$

A non-trivial solution exists only if the acoustic tensor  $\mathbf{Q}$  defined by  $Q_{ik} = D_{ijkl} N_L N_J$  is singular

$$(2.11) \quad \det \mathbf{Q} = 0$$

For this particular process considered here (given by  $\bar{\mathbf{F}} = \mathbf{I} + \alpha \mathbf{G}^0$ ),  $\dot{\bar{\mathbf{F}}}$  is constant and equal to  $\mathbf{G}^0$  and the function  $\Theta(\mathbf{G}^0)$  can be approximated by Eq.5. The tangent stiffness matrix  $\mathbf{D}$  can be numerically approximated by finite differences and becomes (BILBIE et al. [22])

$$(2.12) \quad D_{ijkl} = \frac{\Theta_{ij}(\mathbf{G}^0 + \varepsilon \Delta^{kl}) - \Theta_{ij}(\mathbf{G}^0)}{\varepsilon},$$

$$(2.13) \quad D_{ijkl} = \frac{P_{ij}(\alpha^{n+1} + \delta f \Delta \alpha + \varepsilon \Delta^{kl}) - P_{ij}(\alpha^{n+1} + \delta f \Delta \alpha)}{\delta f \varepsilon \Delta^{kl}},$$

where  $\Delta^{kl}$  is a second-order tensor such that all its components are equal to 0 except the  $kl$  one which is equal to 1,  $\delta f \Delta \alpha$  is a small variation step in the main direction and  $\varepsilon \Delta^{kl}$  is a small perturbation in the direction  $kl$ . In Fig. 3, the stress at the point  $\delta f \Delta \alpha$  (in the same linear direction as the point  $n$ ) and stresses in points with perturbations  $\varepsilon \Delta^{kl}$  are shown.

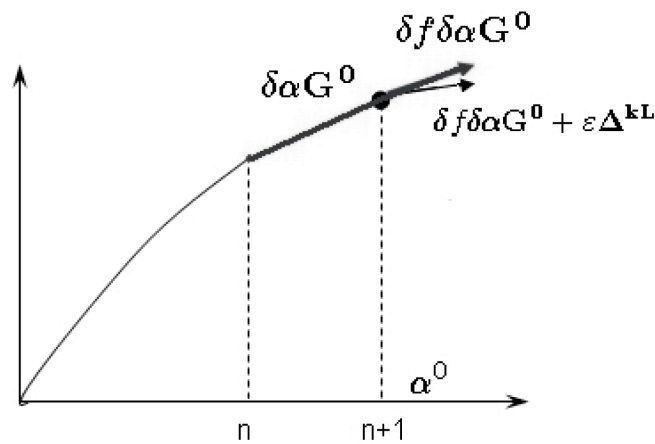


Fig. 3. Schematic computation representation of tangent stiffness matrix.

Rys. 3. Schemat obliczenia stycznej macierzy sztywności

### 3. DISCRETE APPROACH AT MICRO-SCALE

At the macro-scale, the granular system consists for the sake of simplicity of  $N$  polydisperse discs with random radii homogeneously distributed between  $R_{\max} = 5$  mm and  $R_{\min} = 2$  mm. This system is simulated using a discrete element method with a third-order predictor-corrector scheme (ALLEN and TILDESLEY [24]). All discs interact via a linear elastic law and Coulomb friction in contact (CUNDALL and STRACK [25]). The normal contact force  $f_n$  is related to the normal displacement  $\delta$  of the contact as  $f_n = k_n \delta$ , where  $k_n$  is the normal stiffness coefficient ( $\delta > 0$  if a contact is present,  $\delta = 0$  if there is no contact). The tangential component  $f_t$  of the contact force is proportional to the tangential elastic relative displacement with the tangential stiffness coefficient  $k_t$ . The Coulomb condition  $|f_t| \leq \mu f_n$  requires an incremental evaluation of  $f_t$  in each time step leading to some amount of slip each time if one of the equalities  $f_t = \pm \mu f_n$  is imposed ( $\mu=0.5$  – inter-particle friction coefficient). A normal viscous component opposing the relative normal motion of any pair of grains in contact is also added to the elastic force  $f_n$  to obtain a critical damping of the dynamics. The contact normal stiffness  $k_n$  is calculated according to the dimensionless 2D stiffness parameter  $\kappa = k_n/\sigma_0=1000$  denoting the level of the contact deformation  $\kappa = a/ \langle \delta \rangle$ , where  $a$  is the mean diameter of discs and  $\langle \delta \rangle$  is the mean overlap of all grains (COMBE and ROUX [26], ROUX and COMBE [27], ROUX and CHEVOIR [28]). The assumption  $\kappa=1000$  implies that grains can be considered as rigid ones. This value corresponds to the granular material used in experimental tests at Grenoble University (CALVETTI et al. [29], CHARALMPIDOU et al. [30]). The tangential stiffness  $k_t$  can be expressed as a fraction of the normal stiffness  $\bar{k} = k_t/k_n$  with the stiffness ratio  $\bar{k} > 0$  (the ratio  $\bar{k} > 1$  produces the negative Poisson's ratio of grain assemblies, BATHURST and ROTHENBURG [31], CAMBOU et al. [32], EMERIAULT et al. [33]). After several numerical simulations with the different ratios  $\bar{k} \in (0, 1 >$ , the macroscopic behaviour remains similar if  $0.5 \leq \bar{k} \leq 1$ . In this work the ratio  $\bar{k}$  was taken as 1.

A periodic limit condition (PLC) scheme is considered (Fig. 4), where each disc is in contact with neighbours in the simulated cell (primary box) and with some discs in the 'image cell' which are replicated to infinity by rigid translations in 2D Cartesian directions. These replicas contain the same sets of discs as the primary cell (ELLERO [34]). Finally, if one disc moves out of the primary cell, it appears on the opposite side of the cell with the same velocity and opposite momentum.

### 4. MICRO-SCALE STABILITY

Some simple tests for checking the solution stability at the macro-level by checking the acoustic tensor (Eq.11) were performed with 400, 1024, 3025 and 4900 grains, respectively (biaxial test with and without volume changes, oedometer test and shear test). All specimens were initially loaded by the 2D isotropic stress  $\sigma_0$ .

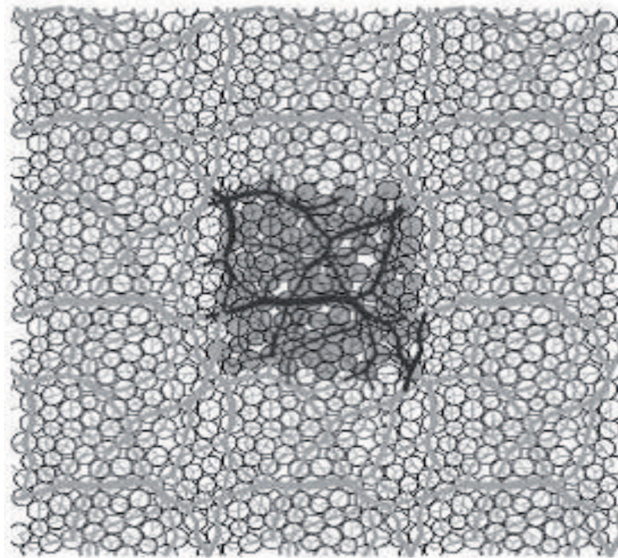


Fig. 4. Shape of periodic limit condition (PLC) specimen with normal contact forces.  
Rys. 4. Kształt próbki dla periodycznych warunków brzegowych (PWB) z normalnymi siłami kontaktowymi

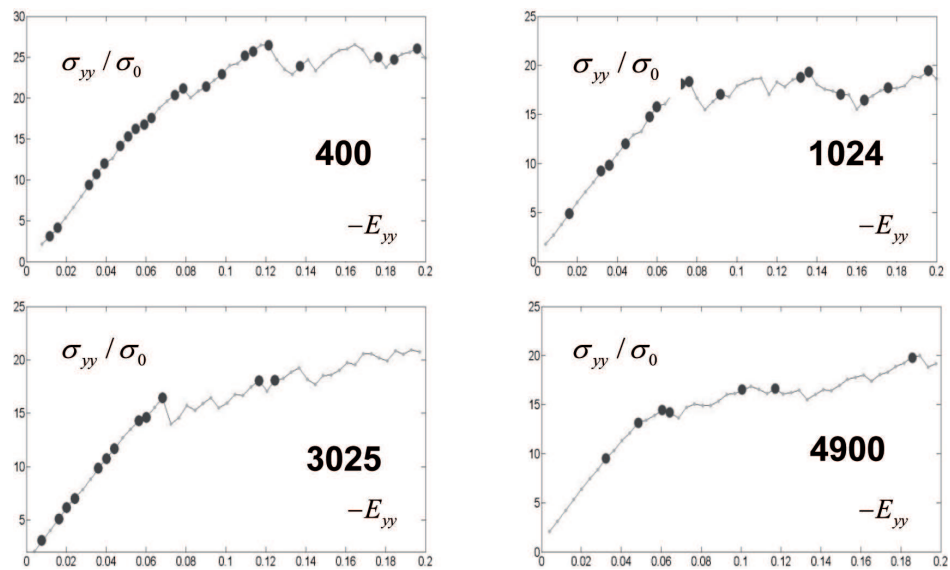


Fig. 5. Influence of specimen size on macroscopic stability during biaxial test ( $\sigma_{yy}$  – vertical normal stress,  $E_{yy}$  – vertical normal strain, ‘-’ – compression).

Rys. 5. Wpływ wielkości próbki na makroskopową stabilność podczas testu dwuosiowego ( $\sigma_{yy}$  – pionowe naprężenie normalne,  $E_{yy}$  – pionowe odkształcenie normalne, ‘-’ – ściskanie)

The influence of the specimen size on the vertical normal stress  $\sigma_{yy}$  is presented in Fig. 5 during biaxial compression (black points (\*) represent instability zones that correspond to  $\det \mathbf{Q} < 0$ ). This test was carried out for the small variation step  $\delta f = 0.01$  and perturbation  $\varepsilon \Delta^{kL} = 2 \cdot 10^{-5}$ . The inertial number was  $I = \dot{\varepsilon} \sqrt{\frac{\langle m \rangle}{\sigma_0}}$  and was assumed between  $1.2 \cdot 10^{-3}$  and  $2.1 \cdot 10^{-3}$  for iterations, and between  $1.2 \cdot 10^{-4}$  and  $2.1 \cdot 10^{-4}$  for variation steps  $\delta f \delta \alpha$ . If both the specimen size increases and the grain number increases, more stable zones are obtained (the number of instabilities decreases) (Fig. 6). More stable zones (less bifurcation points) denote obviously a more stable computation at the macroscopic level.

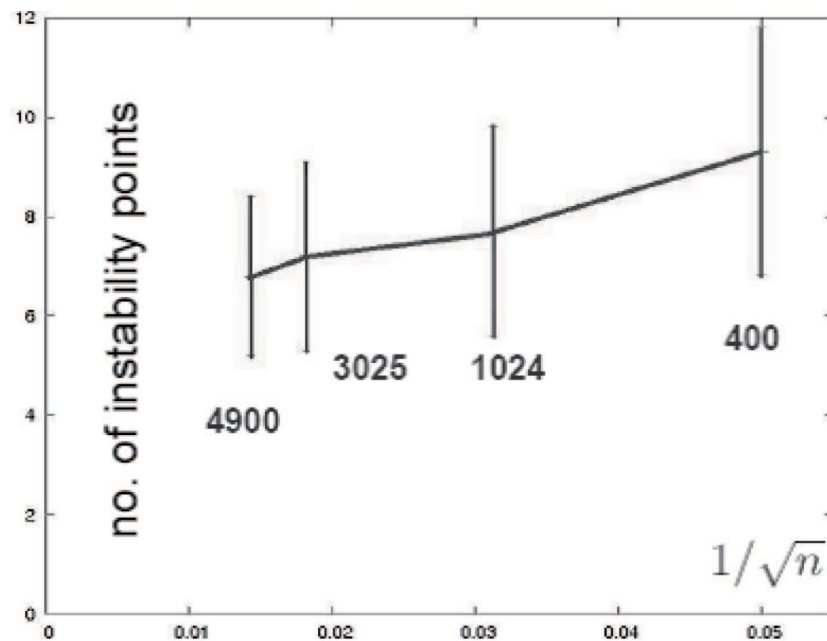


Fig. 6. Influence of specimen size on instabilities during shear test (the instability number versus function of the inverse of the square root of the grain number at strain smaller than 10%).

Rys. 6. Wpływ wielkości próbki na niestabilności podczas testu ścinania (liczba punktów niestabilnych w funkcji odwrotności pierwiastka liczby ziaren w próbce dla odkształcenia mniejszego niż 10%)

Figures 7 and 8 show the influence of the variation step  $\delta f \delta \alpha$  and perturbation  $\varepsilon \Delta^{kL}$  during a biaxial test with 3025 discs. First, the perturbation was taken as  $2 \cdot 10^{-6}$  and the variation step  $\delta f$  varied between 0.05 and 1 (Fig. 7). Next, the variation step was equal to 0.01 and the perturbation step changed between  $2 \cdot 10^{-6}$  and  $2 \cdot 10^{-3}$  (Fig. 8). The larger numbers of stability zones for smaller variation steps and perturbation values were obtained. It is also important to assume a realistic value of  $\delta f \delta \alpha$  to be still in an elasto-plastic regime (not only in an elastic one).

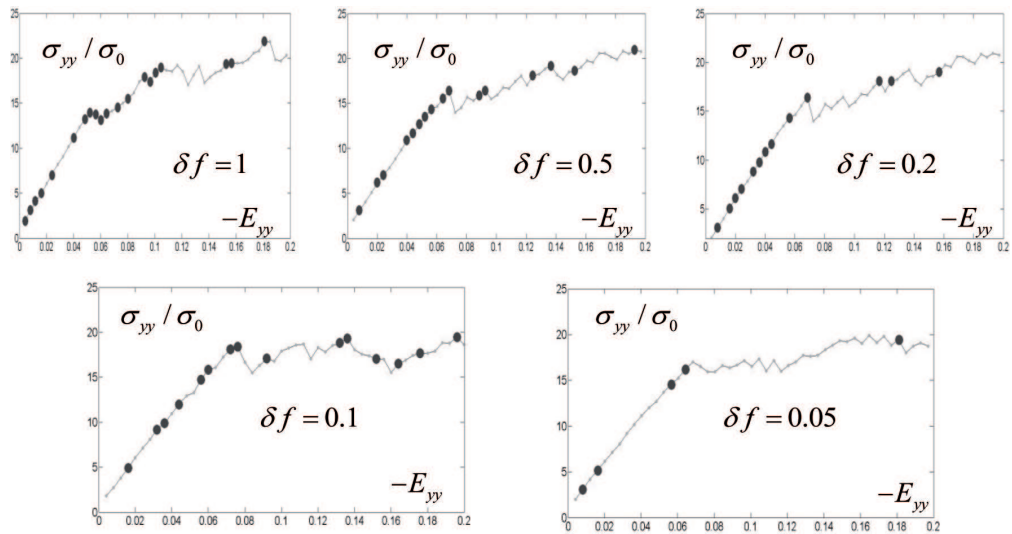


Fig. 7. Influence of variation step on macroscopic stability ( $\sigma_{yy}$  – vertical normal stress,  $E_{yy}$  – vertical normal strain).

Rys. 7. Wpływ kroku zmienności na makroskopową stabilność ( $\sigma_{yy}$  – pionowe napężenie pionowe,  $E_{yy}$  – pionowe odkształcenie normalne)

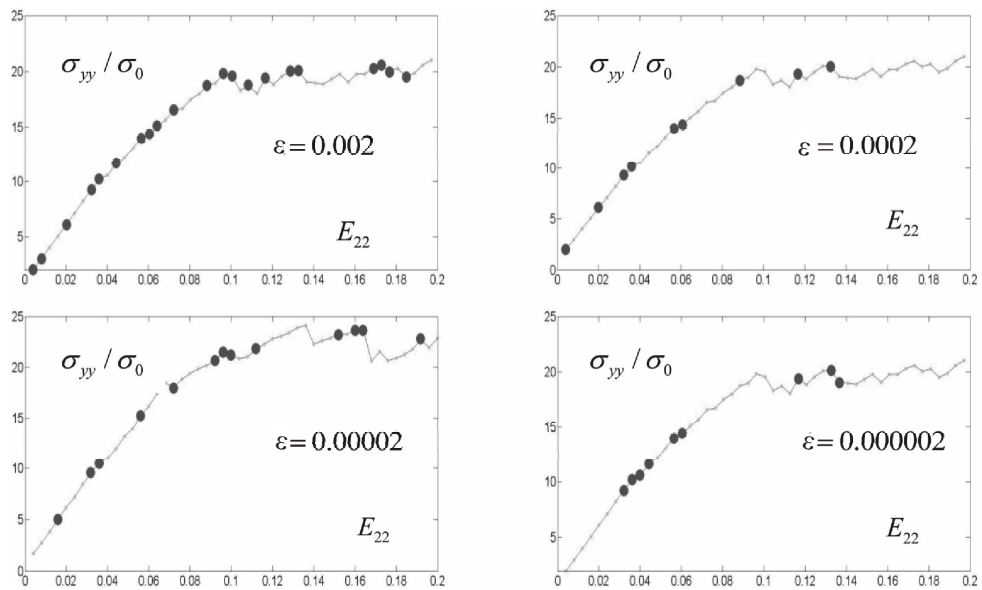


Fig. 8. Influence of perturbation on macroscopic stability ( $\sigma_{yy}$  – vertical normal stress,  $E_{yy}$  – vertical normal strain).

Rys. 8. Wpływ perturbacji na makroskopową stabilność ( $\sigma_{yy}$  – pionowe napężenie normalne,  $E_{yy}$  – pionowe odkształcenie normalne)

## 5. NUMERICAL RESULTS FOR COMBINED DEM-FEM COMPUTATIONS

The DEM-FEM method is implemented in the FEM code *FlagsHyp* (BONNET and WOOD [21]) what involved significant modifications. A driver routine allows one for generating both the stress response and tangent stiffness operator from discrete simulations (according to Section 2). The 2D quadratic element with four Gauss points is chosen. A very simple mesh with 4 elements is used. On the micro level, in DEM calculations, the grain number of in the REV cell is 400. The equilibrium condition is satisfied when the residual  $R < 10^{-5}$  to avoid numerical noises. In DEM calculations, based on our instability study, the variation step  $\delta f$  and perturbation  $\varepsilon$  are chosen as 0.01 and  $2 \cdot 10^{-5}$ , respectively. Initially, REV is assigned an isotropic stress state by compression at the microscopic scale under a kinematic control up to a certain stress. Accordingly, the stress state in each integration point of FE elements is equal to the microscopic stress and the boundary stress is equal to the stress controlled boundaries. The macroscopic stress in each Gauss point equals the microscopic response  $\Sigma_{ij} = \sigma_{ij}$ , where  $\Sigma_{ij}$  is the macroscopic stress and  $\sigma_{ij}$  is the microscopic stress. Along the macroscopic boundary, the isotropic compression is applied to balance the microscopic stresses.

Different numerical tests are performed with a two-scale technique by modelling typical laboratory geotechnical experiments like an oedometric, a biaxial tests and a shear test. All macroscopic results are compared to direct DEM computations on one periodic assemblage of 2D disks (specimen with 400 and 4900 discs).

First, an oedometric test is considered (Fig. 9). The lateral boundaries are fixed and frictionless and the top is displaced downward. The vertical stress increases indefinitely since this path does not lead to plastic flow and the grain degradation is not taken into account. For the isotropic case, the earth pressure ratio  $K_0 = \sigma_{xx}/\sigma_{yy}$  can be related to the Poisson ratio  $\nu$  through  $K_0 = \nu/(1 - \nu)$ . The calculated  $K_0$ -value of 0.40-0.50 corresponds well to cohesionless soils (WU [35], CASTELLANZA et al. [36]). The agreement between macroscopic results by DEM and two-scale ones by DEM-FEM is perfect.

Next, a biaxial test under drained conditions is considered. A constant pressure  $\sigma_0$  is applied to lateral sides, while the top is displaced downward. Using the symmetry of the problem, only the upper left quarter of the specimen is taken into account. The bottom is ideally smooth or has friction. The case with a smooth bottom in Fig. 10 shows typical a biaxial compression response with hardening, peak and softening on the stress-strain curve and volumetric strain curve exhibiting initially small contractancy and then strong dilatancy. The calculated values from the two-scale DEM-FEM analysis are again similar to discrete ones. In turn, the response of the specimen in the case with friction is significantly perturbed on the specimen ends (the lower and earlier peak stress and delayed dilatancy) and departs evidently from the pure discrete response. This was expected, since the latter belongs definitely to a heterogeneous boundary value problem at the macroscopic scale and differs essentially from the elementary response given by the DEM.

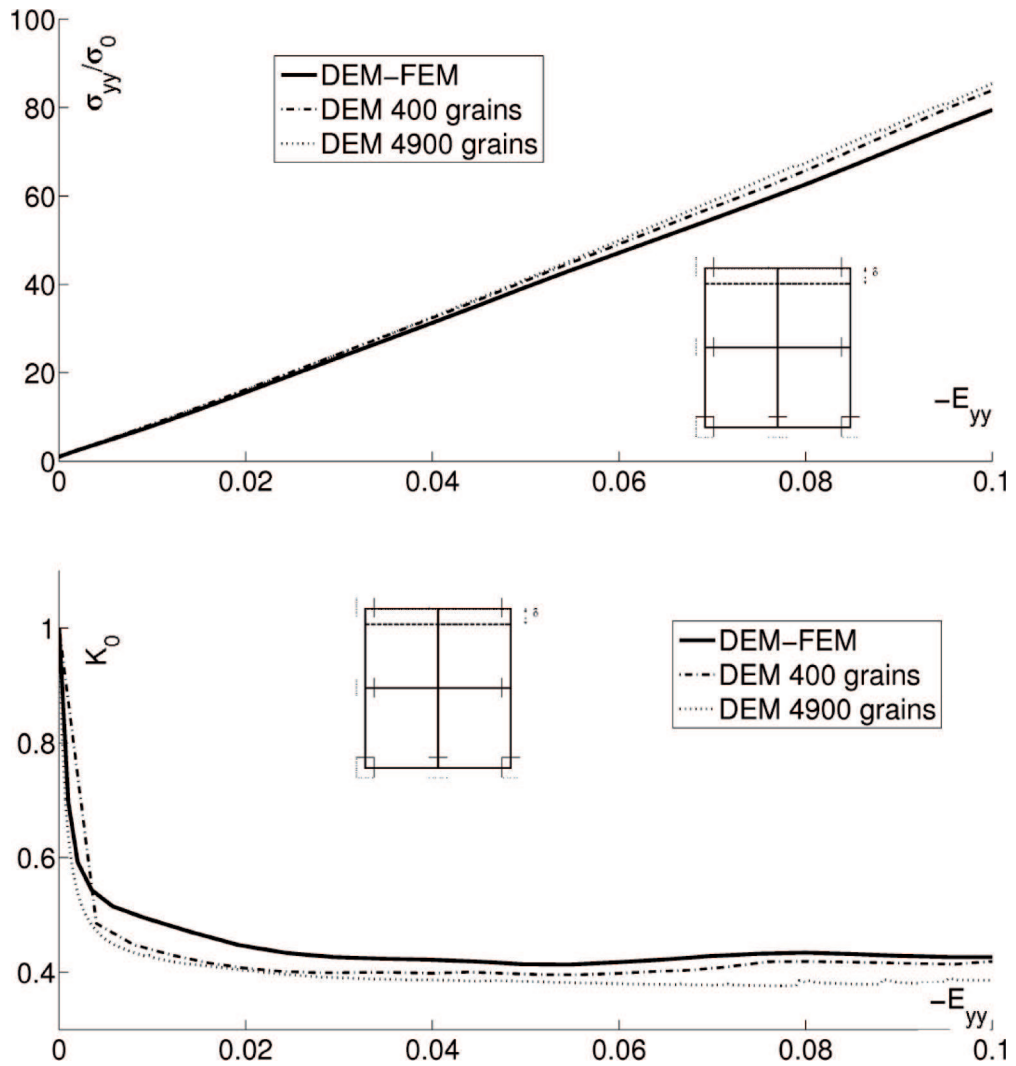


Fig. 9. Two-scale computations of oedometric test for granular materials ( $\sigma_{yy}$  – vertical normal stress,  $\sigma_{xx}$  – horizontal normal stress,  $E_{yy}$  – vertical normal strain,  $K_0 = \sigma_{xx}/\sigma_{yy}$  – the lateral earth pressure coefficient).

Rys. 9. Dwuskalowe obliczenia testu edometrycznego dla materiałów granulowanych ( $\sigma_{yy}$  – pionowe naprężenie normalne,  $\sigma_{xx}$  – poziome naprężenie normalne,  $E_{yy}$  – pionowe odkształcenie normalne,  $K_0 = \sigma_{xx}/\sigma_{yy}$  – współczynnik parcia bocznego gruntu)

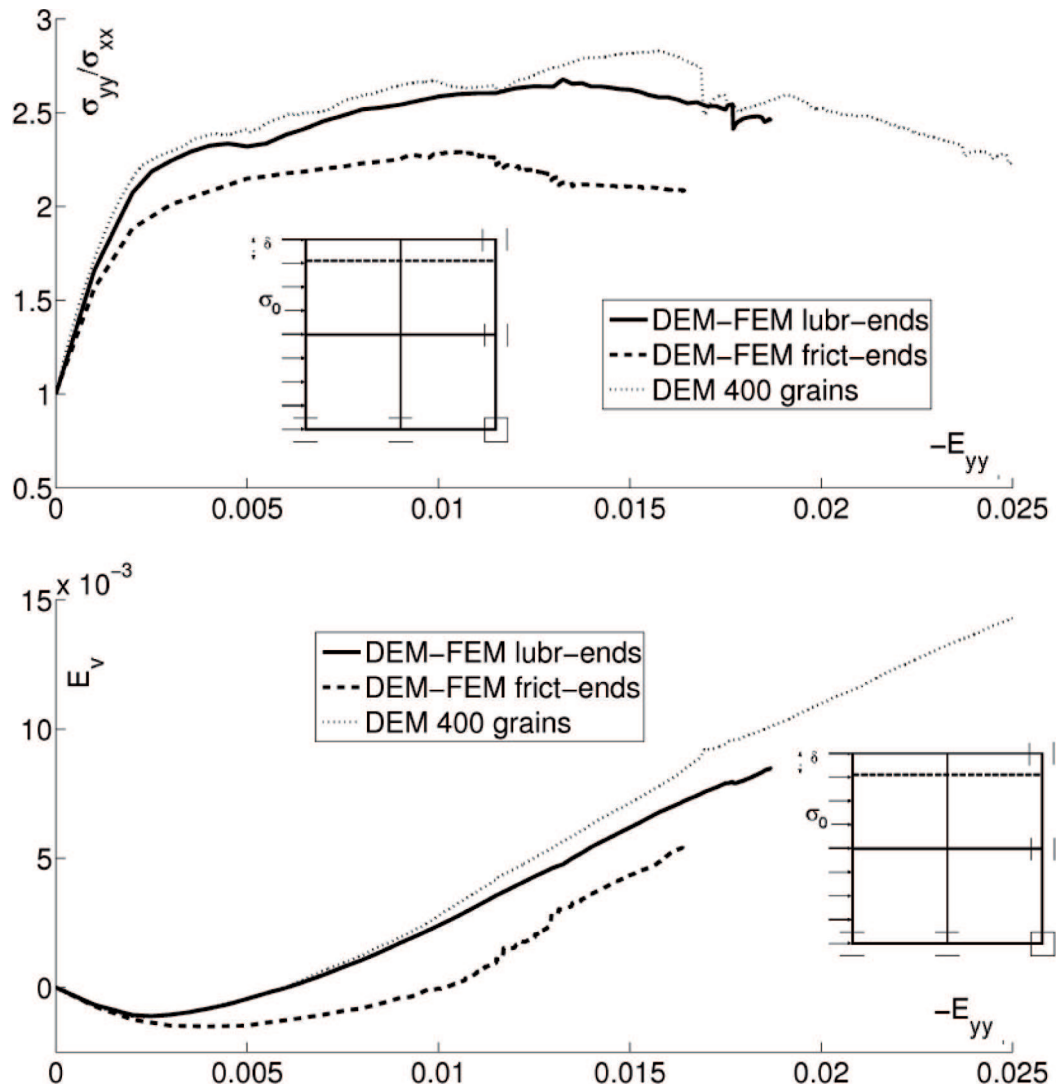


Fig. 10. Two-scale computations of usual biaxial test for granular materials ( $\sigma_{yy}$  – vertical normal stress,  $E_{yy}$  – vertical normal strain,  $E_v$  – volumetric strain).

Rys. 10. Dwuskalowe obliczenia konwencjonalnego testu dwuosowego dla materiałów granulowanych ( $\sigma_{yy}$  – pionowe naprężenie normalne,  $E_{yy}$  – pionowe odkształcenie normalne,  $E_v$  – odkształcenie objętościowe)

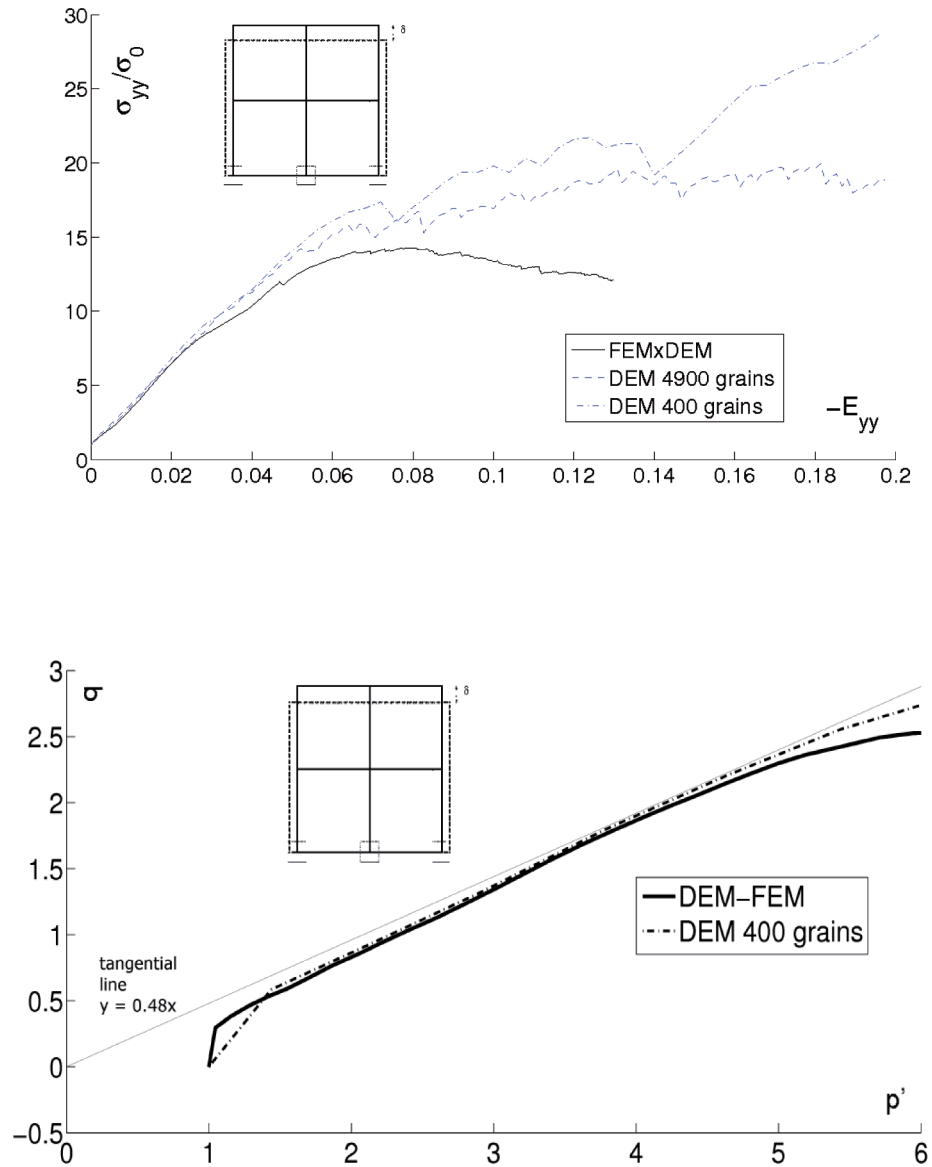


Fig. 11. Two-scale computations of biaxial test without volume changes for granular materials ( $\sigma_{yy}$  – vertical normal stress,  $\sigma_{xx}$  – horizontal normal stress,  $E_{yy}$  – vertical normal strain,  $q$  – deviatoric stress,  $p'$  – mean effective stress).

Rys. 11. Dwuskalowe obliczenia testu dwuosiowego bez zmian objętości dla materiałów granulowanych ( $\sigma_{yy}$  – pionowe naprężenie normalne,  $\sigma_{xx}$  – poziome naprężenie normalne,  $E_{yy}$  – pionowe odkształcenie normalne,  $q$  – naprężenie dewiatorowe,  $p'$  – średnie naprężenie efektywne)

Next, the calculations are carried out with biaxial compression without volume changes (Fig. 11). The specimen is subjected to compression from the top and extension from both sides. In the calculations, the stress path reaches shortly a straight line, and then goes up along this line due to the constrained dilatancy that strongly increases the mean effective stress.

Finally, the results for a shear test are presented (Fig. 12). The top wall is moved into the X-axis direction with the isotropic pressure  $\sigma_0$  applied to the boundary. First, the ratio between the deviatoric stress and mean effective stress  $q/p'$  rapidly increases and then reaches an asymptote. In combined DEM-FEM calculations, the ratio  $q/p'$  is slightly smaller than in pure DEM ones.

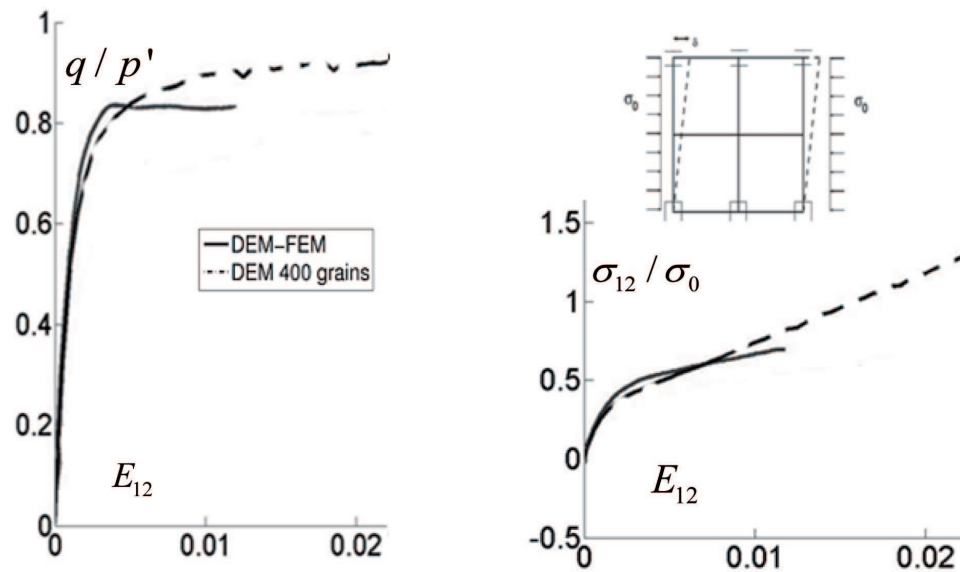


Fig. 12. Two-scale computations of shear test for granular materials ( $q$  – deviatoric stress,  $p'$  – mean effective stress,  $\sigma_{12}$  – shear stress,  $E_{12}$  – shear strain).

Rys. 12. Dwuskalowe obliczenia testu ścinania dla materiałów granulowanych ( $q$  – napężenie dewiatorowe,  $p'$  – średnie napężenie efektywne,  $\sigma_{12}$  – napężenie styczne,  $E_{12}$  – odkształcenie styczne

## 6. CONCLUSIONS

A two-scale numerical approach for granular materials was proposed combining the DEM simulation of the granular micro-structure at the micro-level with the FEM modelling of the overall material response at the macro-level.

The results show that the continuum tangent matrix at the macroscopic may provide an unstable solution if the REV sample at the microscopic level behaves as a discrete medium. Thus, a correct choice for the specimen size, grain number, variation step

and perturbation value is of major importance to reduce numerical instabilities at the micro-scale level and to ensure a stable solution at the macro-level. The solution stability increases with increasing specimen size and number of discs. In an unstable regime, some grains lose their contacts for different variation steps and perturbations. Such microscopic behaviour may be truly physical linked to shear banding. However, the occurrence of such instabilities far from the failure regime in numerous points of the load-displacement diagram may indicate a non-relevant numerical behaviour and therefore has to be minimized.

The combined DEM-FEM computations with a numerically calculated tangent stiffness matrix work well for simple loading cases in spite of the occurrence of unstable points. The results are similar to those obtained from DEM computations and qualitatively similar to the corresponding laboratory tests. They give a faster response for large geotechnical problems than DEM. However, for more complex BV problems, the proposed two-scale approach may fail.

Our research will be continued for granular materials by including strain localization. To model the grain roughness, contact moments will be used at discs at the micro-level (Widuliński et al. [37]). To obtain a stable solution at the macro-level and to eliminate unstable points, a non-local approach will be used at the micro-level for calculating the tangent stiffness matrix (Tejchman [38]). The results will be again checked by pure discrete simulations.

## 7. ACKNOWLEDGEMENT

Research work was carried out by the first author during his stay at Grenoble University within the research grant ANR in Laboratoire 3S-R

Research work was carried out by the second author as a part of the project: “Innovative ways and effective methods of safety improvement and durability of buildings and transport infrastructure in the sustainable development” financed by the European Union.

## REFERENCES

1. C. MIEHE, J. SCHOTTE, J. SCHRÖDER, *Computational homogenization analysis in finite plasticity. Simulation of texture development in polycrystalline materials*. Computer Methods in Applied Mechanics and Engineering **171**, 387-418, 1999.
2. F. FEYEL, J.L. CHABOCHE, *FE2 multiscale approach for modelling the elastoviscoplastic behaviour of long fiber SiC/Ti composite materials*. Computer Methods in Applied Mechanics and Engineering **183**, 309-330, 2000.
3. K. TERADA, N. KIKUCHI, *Nonlinear homogenization method for practical applications*. Computational Methods in Micromechanics (eds. S. Ghosh and M. Ostoja-Starzewski), 1-16, 1995.
4. S. GHOSH, K. LEE, S. MOORTHY, *Multiple scale analysis of heterogeneous elastic structures using homogenisation theory and Voronoi cell finite element method*. International Journal for Solids and Structures **32**(1), 27-62, 1995.

5. V. G. KOUZNETSOVA, M. GEERS, W. A. M. BREKELMANS, *Size of representative volume element in a secondorder computational homogenization framework*. International Journal for Multiscale Computational Engineering **2**(4), 575-598, 2004.
6. I. M. GITMAN, H. ASKES, L.J. SLUYS, *Coupled volume multiscale modelling of quasibrittle material*. European Journal of Mechanics A/Solids **27**(3), 302-327, 2008.
7. T.J. MASSART, V. KOUZNETSOVA, R.H.J. PEERLINGS, M.G.D. GEERS, *Computational Homogenization for Localization and Damage*. Advance Computational Materials Modelling: From Classical to Multi-scale Techniques (eds.: M. Vaz Júnior, E. A. de Souza Neto, P. A. Muñoz-Rojas), 2010.
8. J.C. MICHEL, H. MOULINEC, P. SUQUET, *Effective properties of composite materials with periodic microstructure: a computational approach*. Computer Methods in Applied Mechanics and Engineering **172**, 109-143, 1999.
9. A. HUND, E. RAMM, *Locality constraints within multiscale model for nonlinear material behaviour*. International Journal for Numerical Methods in Engineering **70**(13), 1613-1632, 2007.
10. S. ECKARDT, C. KÖNKE, *Adaptive damage simulation of concrete using heterogeneous multiscale models*. Journal of Algorithms and Computational Technology **2**(2), 275-297, 2008.
11. A. IBRAHIMBEGOVIC, D. MARKOVIC, F. GATUNGT, *Constitutive model of coupled damageplasticity and its finite element implementation*. European Journal of Computational Mechanics **12**(4), 381-405, 2003.
12. Ł. KACZMARCZYK, C.J. PEARCE, N. BICANIC, E. DE SOUZA NETO, *Numerical multiscale solution strategy for fracturing heterogeneous materials*. Computer Methods in Applied Mechanics and Engineering **199**, 1100-1113, 2009.
13. R. HILL, *Elastic properties of reinforced solids: Some theoretical principles*. Journal of the Mechanics and Physics of Solids **11**(5), 357-372, 1963.
14. P. EVESQUE, *Fluctuations, correlations and representative elementary volume (REV) in granular materials*. Powders and Grains **11**, 6-17, 2000.
15. I.M. GITMAN, *Representative volumes and multi-scale modelling of quasi-brittle materials*. PhD thesis, Delft University of Technology, 2006.
16. Ł. SKARŻYŃSKI, J. TEJCHMAN, *Mesosopic modelling of strain localization in concrete*. Archives of Civil Engineering LV **4**, 503-526, 2009.
17. Ł. SKARŻYŃSKI, J. TEJCHMAN, *Determination of representative volume element in concrete under tensile deformation*. Computers and Concrete, 2011 (in print).
18. M. NITKA, *Modelisation multi-echelle des milieux granulaires (Multiscale modeling of granular media)*, PhD Thesis, University of Grenoble, 2010.
19. M. NITKA, G. COMBE, C. DASCALU, J. DESRUES, *Two-scale modeling of granular materials: a DEM-FEM approach*. Granular Matter **13**, 277-281, 2011.
20. A.E.H. LOVE, *A treatise on the mathematical theory of elasticity*. Cambridge University Press, 217-236; 1927.
21. J. BONNET, R.D. WOOD, *Nonlinear continuum mechanics for finite element analysis*. Cambridge University Press, 53-117, 1997.
22. G. BILBIE, C. DASCALU, R. CHAMBON, D. CAILLERIE, *Micro-fracture instabilities in granular solids*. Acta Geotechnica **3**, 25-35, 2008.
23. J.R. RICE, *The localization of plastic deformation*. Theoretical and Applied Mechanics, W.T. Koiter, ed., North-Holland Publishing Company, 207-220, 1976.
24. M.P. ALLEN, TILDESLEY, *Computer simulation of liquids*. Oxford Science Publications, 1994.
25. P.A. CUNDALL, O.D.L. STRACK, *A discrete numerical model for granular assemblies*; Geotechnique **29**, 1, 47-65, 1979.
26. G. COMBE, J.-N. ROUX, *Discrete numerical simulation, quasistatic deformation and the origins of strain in granular materials*. Proc. 3rd International Symposium on Deformation Characteristics of Geomaterials, Lyon, France (H. DiBenedetto, T. Doanh, H. Geoffroy, C. Sauzeat, eds.), 1071-1078, 2003.

27. J.-N. ROUX, G. COMBE, *On the meaning and microscopic origins of quasistatic deformation of granular materials*. Proc. 16th ASCE Engineering Mechanics Conference, 2003.
28. J.-N. ROUX, F. CHEVOIR, *Discrete numerical simulation and the mechanical behaviour of granular materials*. Bulletin des Laboratoires des Ponts et Chaussées **254**, 109-138, 2005.
29. F. CALVETTI, G. COMBE, J. LANIER, *Experimental micromechanical analysis of a 2D granular material: relation between structure evolution and loading path*. Mechanics of Cohesive-Frictional Materials **2**, 121-163, 1997.
30. E.-M. CHARALMPIDOU, G. COMBE, G. VIGGIANI, J. LANIER, *Mechanical observations on dense 2D granular media*. Powders and Grains, Colorado, USA, 2009.
31. J. BATHURST, L. ROTHENBURG, *Micromechanical aspects of isotropic granular assemblies with linear contact interactions*. Journal of Applied Mechanics **55**, 17-23, 1988.
32. B. CAMBOU, P. DUBUJET, F. EMERIAULT, F. SIDOROFF, *Homogenization for granular materials*. European Journal of Mechanics Solids **14**, 255-276, 1995.
33. B. EMERIAULT, B. CAMBOU, A. MAHBOUDI, *Homogenization for granular materials: non reversible behavior*. Mechanics of Cohesive-Frictional Materials **1**, 199-218, 1996.
34. M. ELLERO, *Smoothed particle dynamics methods for the simulation of viscoelastic fluids*. Thesis, Berlin University, 3-10, 2004.
35. W. WU, *Hypoplastizität als mathematisches Modell zum mechanischen Verhalten granularer Stoffe*. Heft 129, Institute for Soil- and Rock-Mechanics, University of Karlsruhe, 1992.
36. R. CASTELLANZA, R. NOVA, M. ARROYO, *Oedometric testing and compaction bands in cemented soils*. Soils and Foundations **45**, 2, 181-194, 2005.
37. L. WIDULINSKI, J. TEJCHMAN, J. KOZICKI, D. LEŚNIEWSKA, *Discrete simulations of shear zone patterning in sand in earth pressure problems of a retaining Wall*. Int. J. Solids and Structures **48**, 7-8, 1191-1209, 2011.
38. J. TEJCHMAN, *Influence of a characteristic length on shear zone formation in hypoplasticity with different enhancements*. Computers and Geotechnics **31**, 8, 595-611, 2004.

## DWUSKALOWE NUMERYCZNE PODEJŚCIE DO SYSTEMÓW GRANULOWANYCH

### Streszczenie

Zastosowano dwuskalowe numeryczne podejście homogenizacyjne do materiałów granulowanych. Na poziomie małej skali symulowano granulowaną mikrostrukturę przy zastosowaniu metody elementów dyskretnych. Na poziomie dużej skali zastosowano metodę elementów skończonych. Technika przechodzenia do wyższej skali uwzględniła dyskretny model w każdym punkcie całkowania Gaussa siatki MES w celu wyprowadzenia numerycznego obliczenia wynikowej konstytutywnej odpowiedzi materiału. W tym procesie, operator styczny został obliczony za pomocą przyrostu naprężenia odpowiadającego danemu przyrostowi odkształcenia w punkcie Gaussa. W celu wykrycia utraty jednoznaczności rozwiązania, określono wyznacznik tensor akustycznego związanego z operatorem stycznym. Obliczono numerycznie kilka podstawowych testów geotechnicznych stosując połączoną technikę MED-MES.

*Remarks on the paper should be sent to the Editorial Office no later than December 30, 2011*

*Received April 18, 2011  
revised version  
August 5, 2011*